Molecular Basis for P-Site Inhibition of Adenylyl Cyclase[†,‡]

John J. G. Tesmer,[§] Carmen W. Dessauer,[||] Roger K. Sunahara,[⊥] Leyton D. Murray,[#] Roger A. Johnson,[#] Alfred. G. Gilman, and Stephen R. Sprang*

Department of Chemistry and Biochemistry, University of Texas at Austin, Austin, Texas 78712-1167, Department of Integrative Biology and Pharmacology, University of Texas Medical School, 6431 Fannin Street, Houston, Texas 77030, Howard Hughes Medical Institute, Department of Biochemistry, and the Department of Pharmacology, The University of Texas Southwestern Medical Center at Dallas, 5323 Harry Hines Boulevard, Dallas, Texas 75390-9041, and Department of Physiology and Biophysics, State University of New York, Health Sciences Center, Stony Brook, New York 11794-8661

Received July 5, 2000; Revised Manuscript Received September 1, 2000

ABSTRACT: P-site inhibitors are adenosine and adenine nucleotide analogues that inhibit adenylyl cyclase, the effector enzyme that catalyzes the synthesis of cyclic AMP from ATP. Some of these inhibitors may represent physiological regulators of adenylyl cyclase, and the most potent may ultimately serve as useful therapeutic agents. Described here are crystal structures of the catalytic core of adenylyl cyclase complexed with two such P-site inhibitors, 2′-deoxyadenosine 3′-monophosphate (2′-d-3′-AMP) and 2′,5′-dideoxyadenosine 3′-triphosphate (2′,5′-dd-3′-ATP). Both inhibitors bind in the active site yet exhibit non- or uncompetitive patterns of inhibition. While most P-site inhibitors require pyrophosphate (PP_i) as a coinhibitor, 2′,5′-dd-3′-ATP is a potent inhibitor by itself. The crystal structure reveals that this inhibitor exhibits two binding modes: one with the nucleoside moiety bound to the nucleoside binding pocket of the enzyme and the other with the β and γ phosphates bound to the pyrophosphate site of the 2′-d-3′-AMP·PP_i complex. A single metal binding site is observed in the complex with 2′-d-3′-AMP, whereas two are observed in the complex with 2′,5′-dd-3′-ATP. Even though P-site inhibitors are typically 10 times more potent in the presence of Mn^{2+}, the electron density maps reveal no inherent preference of either metal site for Mn^{2+} over Mg^{2+}. 2′,5′-dd-3′-ATP binds to the catalytic core of adenylyl cyclase with a K_d of 2.4 μM in the presence of Mg^{2+} and 0.2 μM in the presence of Mn^{2+}. Pyrophosphate does not compete with 2′,5′-dd-3′-ATP and enhances inhibition.

Adenylyl cyclase is an integral membrane protein composed of alternating pairs of membrane and cytoplasmic domains. The two major conserved cytoplasmic domains, C_{1a} and C_{2a}, form the catalytic core of the enzyme with the active site at their interface (*1*, *2*). The catalytic core also contains the primary binding sites for activators of adenylyl cyclase such as $G_s\alpha$[1] and the diterpene forskolin. Early studies demonstrated that adenosine and certain adenosine derivatives could inhibit the production of cAMP in intact cells (*3*). Such analogues required the presence of an intact adenine ring (*4*), and their locus of action has been designated the "P"-site. The locus for P-site inhibition was eventually established to be on adenylyl cyclase itself (*5*−*9*) and, more specifically, localized to the catalytic cleft of the enzyme in studies of purified C_{1a} and C_{2a} domains (*10*). P-site inhibitors occur naturally in vivo, and as such may represent physiological regulators of adenylyl cyclase (*11*, *12*).

Kinetic and structural analysis of P-site inhibition demonstrate that the reaction coordinate of the chemical transformation catalyzed by adenylyl cyclase is complex and involves several conformational states (*13*). P-site inhibitors are not competitive with activators such as Mn^{2+}, forskolin or $G_s\alpha$, and they are much more potent inhibitors of the activated than the basal enzyme (*8*). Inhibition with respect to ATP is typically un- or noncompetitive in the presence of Mg^{2+} or Mn^{2+}, respectively (*13*), but is competitive with respect to cAMP for the reverse reaction and requires the product PP_i (*14*). P-site inhibitors are now believed to form a dead-end complex with adenylyl cyclase by occupying the site that previously accommodated the second product,

[†] R.K.S. was supported by a postdoctoral fellowship from the Medical Research Council of Canada. This work was supported by NIH Grants DK38828 (to R.A.J.) and DK46371 (to S.R.S), by an Innovative Technology Grant from the Stony Brook Center for Biotechnology to R.A.J., by Welch Foundation Grants I-1271 (to A.G.G.) and I-1229 (S.R.S.), and by the Raymond and Ellen Willie Distinguished Chair of Molecular Neuropharmacology (to A.G.G.).

[‡] Research Collaboratory for Structural Bioinformatics Protein Databank filenames 1CS4 and 1CUL.

* To whom correspondence should be addressed at Howard Hughes Medical Institute, Department of Biochemistry, The University of Texas Southwestern Medical Center at Dallas. Phone: (214) 648-5008. Fax: (214) 648-6336. E-mail: sprang@chop.swmed.edu.

[§] University of Texas at Austin.

[||] University of Texas Medical School.

[⊥] Department of Pharmacology, The University of Texas Southwestern Medical Center at Dallas.

[#] State University of New York.

[1] Abbreviations: $G_s\alpha$, the stimulatory G protein α subunit; cAMP, adenosine-3′,5′-cyclic monophosphate; 2′-d-Ado, 2′-deoxyadenosine; 2′-d-3′-AMP, 2′-deoxyadenosine 3′-monophosphate; 2′,5′-dd-3′-ADP, 2′,5′-dideoxyadenosine 3′-diphosphate; 2′,5′-dd-3′-ATP, 2′,5′-dideoxyadenosine 3′-triphosphate; 2′, 5′-dd-3′-A4P, 2′,5′-dideoxyadenosine 3′-tetraphosphate; PP_i, pyrophosphate; AP(CH_2)PP, adenosine 5′-(α,β-methylene)-triphosphate; GTPγS, guanosine 5′-[γ-thio]triphosphate; ATPγS (R_p), adenosine 5′-[α-thio]triphosphate, R_p enantiomer; MES, 2-(*N*-morpholino)-ethanesufonic acid; HEPES, *N*-2-hydroxyethylpiperazine-*N*′-2-ethanesulfonic acid.

10.1021/bi0015562 CCC: $19.00
Published on Web 11/02/2000

cAMP, before PP_i is released (*8*, *14*). Indeed, high-resolution crystal structures show that the P-site inhibitor 2′-d-3′-AMP·PP_i binds to the active site of the enzyme in a manner analogous to that of ATP or, perhaps more accurately, cAMP·PP_i (*2*). Recently, adenosine-3′-polyphosphates have been developed as a new class of P-site inhibitors with enhanced potency (*12*, *15*). Extrapolating from the structure of 2′-d-3′-AMP·PP_i in complex with adenylyl cyclase, it has been proposed that the β and γ phosphates of adenine nucleoside-3′-triphosphates occupy the PP_i binding site (*16*, *17*).

Reported here are biochemical and crystallographic studies aimed at understanding the mechanism of action and metal dependence of P-site inhibitors, in particular the adenine nucleoside-3′-polyphosphates. The biochemical studies examine the mode of inhibition, and the binding constants of 2′,5′-dd-3′-ATP for the catalytic domains of adenylyl cyclase in the presence of either Mg^{2+} or Mn^{2+}, assess the requirement for PP_i and look for competition with adenosine and ATP analogues. Six high-resolution crystal structures are reported: those of adenylyl cyclase with 2′-d-3′-AMP·PP_i or 2′,5′-dd-3′-ATP, each with three different combinations of metal ions. One structure for each P-site inhibited complex is described in detail.

EXPERIMENTAL PROCEDURES

Materials. 2′,5′-dd-3′-ADP and 2′,5′-dd-3′-ATP were synthesized as described previously (*12*, *15*). 2′,5′-dd-[γ-^{32}P]-3′-ATP was synthesized by substrate level phosphorylation from 2′,5′-dd-3′-ADP and $^{32}P_i$.[2] Carrier-free $^{32}P_i$ (orthophosphoric acid, typically 10 mC_i in ~67 μL of water) was from New England Nuclear Corp.

Preparation of Proteins. Canine type V C_{1a} domain, rat type II C_{2a} domain, and bovine $G_s\alpha$ (short form) were synthesized in *Escherichia coli* and purified as described previously (*2*, *18*, *19*). The C_{1a} construct includes an amino-terminal hexahistidine tag. The amino acids included in each construct are as follows: C_{1a}, residues 364−591 for the biochemical analyses and residues 364−580 for the crystallographic analyses; C_{2a}, residues 874−1081; $G_s\alpha$, residues 1−396 (numbering reflects the sequence for the long form of $G_s\alpha$). $G_s\alpha$ was activated by incubation with GTPγS and Mg^{2+} at 35° C for 3 h as described (*20*) to yield GTPγS−$G_s\alpha$. For the crystallographic studies, GTPγS−$G_s\alpha$ was treated with trypsin as described (*19*); the resulting fragment spans residues 39−389.

Adenylyl Cyclase Assays. Synthesis of cAMP was measured for 10 min at 30 °C in a final volume of 100 μL as previously described (*10*). Inhibition kinetics were determined on enzyme assayed with concentration of divalent cation fixed in excess of the ATP concentration as described previously (*14*, *21*).

Equilibrium Dialysis. Equilibrium dialysis was performed essentially as described (*22*). Each chamber contained 20 mM NaHEPES (pH 8.0), 5 mM $MgCl_2$, 2 mM dithiothreitol, 50 mM NaCl, 2′,5′-dd-[γ-^{32}P]-3′-ATP (0.1−12.8 μM), and other additions as indicated. One chamber contained 4 μM active C_{1a}(591), C_{2a}, and GTPγS-$G_{s\alpha}$. The opposite chamber contained buffer in lieu of proteins. Samples were removed after dialysis for 24 h at 4 °C with rotation. Duplicate 15 μL aliquots from each chamber were analyzed by liquid scintillation spectrometry.

Crystallization and Formation of P-Site Complexes. C_{1a}, C_{2a}, and trypsin-treated $G_s\alpha$ were mixed to form a ternary complex in the presence of forskolin (C_{1a}·C_{2a}·$G_s\alpha$) and then purified by gel filtration. Crystals were grown as described previously (*2*). The crystals were then soaked for various lengths of time at room temperature in harvesting solution (10% PEG 8000, 30% PEG 400, 100 mM MES pH 5.6, 20 mM NaHEPES, pH 8.0, 3.33 mM dithiothreitol, 500 mM NaCl, 200 μM 7-deacetyl-7-[*O*-(*N*-methylpiperazino)-γ-butyryl]-forskolin, 166 μM GTPγS) that also contained various combinations of inhibitors and metal ions. For the 2′-d-3′-AMP·PP_i·Mg^{2+} complex, crystals were soaked in harvesting solution that in addition contained 5.5 mM $MgCl_2$, 2.9 mM 2′-d-3′-AMP, and 2.9 mM Na_4PP_i for 1.75 h; for 2′-d-3′-AMP·PP_i·Mn^{2+}, 500 μM $MgCl_2$, 250 μM $MnCl_2$, 2.9 mM 2′-d-3′-AMP, and 2.9 mM Na_4PP_i for 1.5 h; for 2′-d-3′-AMP·PP_i·Zn^{2+}, 500 μM $MgCl_2$, 500 μM $ZnCl_2$, 2.9 mM 2′-d-3′-AMP, and 2.9 mM Na_4PP_i for 1.5 h; for 2′,5′-dd-3′-ATP·Mg^{2+}, 5 mM $MgCl_2$ and 1 mM 2′,5′-dd-3′-ATP for 1 h; for 2′,5′-dd-3′-ATP·Mn^{2+}, 250 μM $MnCl_2$ and 0.5 mM 2′,5′-dd-3′-ATP for 1.5 h; for 2′,5′-dd-3′-ATP·Zn^{2+}, 250 μM $ZnCl_2$ and 1.0 mM 2′,5′-dd-3′-ATP for 1.5 h. Mg^{2+} was present in these last two soaks only in residual amounts, as crystals were grown in the presence of $MgCl_2$.

Structure Determinations. Diffraction maxima from each complex were collected on a 2k × 2k Quantum 4 CCD area detector at beam line F1 at the Cornell High Energy Synchrotron Source (CHESS). The wavelength of the incident beam was 0.921 Å. The data were integrated and reduced using MOSFLM and SCALA of the CCP4 programming suite (*23*). Data collection statistics are shown in Table 1. Initial phases were generated by molecular replacement using the previously reported 2.8 Å resolution structure of adenylyl cyclase in complex with 2′-d-3′-AMP·PP_i with the inhibitor coordinates omitted from the model (*2*). After one round of rigid body refinement, Powell minimization and simulated annealing with the program CNS (*24*), a SIGMAA-weighted $|F_o| - |F_c|$ omit map was generated to locate and fit the inhibitor and metals in each structure. At this point, three difference Fourier maps were calculated for each P-site inhibitor: $|F_{o_{Mn}}| - |F_{o_{Mg}}|$, $|F_{o_{Zn}}| - |F_{o_{Mg}}|$ and $|F_{o_{Mn}}| - |F_{o_{Zn}}|$, where $|F_{o_{Mg}}|$, $|F_{o_{Mn}}|$, and $|F_{o_{Zn}}|$ are the observed structure factor amplitudes for crystals of the Mg^{2+}, Mn^{2+}, and Zn^{2+} complexes, respectively. Because these maps revealed no significant differences among the three data sets, only the data sets judged to be the best for each inhibitor, based on the quality of the data (merging *R* factor and $\langle I\rangle/\langle\sigma_I\rangle$) and electron density map, (2′-d-3′-AMP·PP_i·Zn^{2+} and 2′,5′-dd-3′-ATP·Mn^{2+}) were used in subsequent refinement of the respective models by alternating rounds of Powell minimization, individual *B*-factor refinement, and model building. In each of these models, both metal A and metal B were refined as Mg^{2+}. Anisotropic overall *B*-factors and a bulk solvent mask were used throughout refinement. For the 2′,5′-dd-3′-ATP·Mn^{2+} data set, the inhibitor electron density was modeled as a molecule of 2′,5′-dd-3′-AMP and a triphosphate group. The 3′ phosphate of 2′,5′-dd-3′-AMP and the α phosphate of the triphosphate occupy the same position in this model. The occupancies of these two groups

[2] [2]R. A. Johnson, unpublished observation.

Table 1: Summary of Data Collection and Refinement Statistics[a]

crystal	2d3AMP·Mg	2d3AMP·Mn	2d3AMP·Zn	dd3ATP·Mg	dd3ATP·Mn	dd3ATP·Zn
cell constants (Å)						
a	118.6	118.5	118.5	118.6	118.2	118.0
b	134.0	134.4	134.5	134.6	133.6	133.9
c	70.9	71.1	71.3	71.8	70.6	70.8
no. of crystals	1	1	1	1	1	1
D_{min} (Å, along ***a**** and ***b****)	2.9	2.8	2.5	2.8	2.4	2.5
unique reflections	22 650	16 552	39 407	27 520	36 169	39 186
avg redundancy	2.8	3.6	3.0	3.4	2.7	3.4
R_{sym}[b] (%)	13.6	9.1	10.9	13.1	11.7	14.3
completeness (%)	88.7	60.4	98.4	95.2	82.4	99.0
$\langle I\rangle/\langle\sigma_I\rangle$	5.0	7.1	6.1	4.4	5.4	4.3
resolution range for refinement (Å)[c]			15−2.5		15−2.4	
total reflections used			36 050		32 910	
no. protein atoms			5647		5641	
no. water molecules			77		83	
no. heterogen atoms			119		124	
rmsd bond lengths (Å)			0.007		0.007	
rmsd bond angles (deg)			1.22		1.22	
rmsd bonded *B*-factors (Å^2)			2.45		2.80	
R_{work}[d] (%)			21.6		21.6	
R_{free}[e] (%)			26.4		26.3	
avg *B*-factor (Å^2)			50.9		48.4	

[a] Table abbreviations: 2d3AMP, 2′-d-3′-AMP; dd3ATP, 2′,5′-dd-3′-ATP. [b] $R_{sym} = \sum_h\sum_i |I(h) - I(h)_i|/\sum_h\sum_i I(h)_i$ where $I(h)$ is the mean intensity after rejections. [c] Due to anisotropy, data with an l index greater than 20 were omitted from refinement. [d] $R_{work} = \sum_h||F_o(h)| - |F_c(h)||/\sum_h|F_o(h)|$, where $F_o(h)$ and $F_c(h)$ are observed and computed structure factors; no I/σ cutoff was used during refinement. [e] 10% of the complete data set was excluded from refinement to calculate R_{free}.

were set to 50%, and the van der Waals interaction terms between them were omitted during refinement. No residues from either model exhibited main chain conformations corresponding to disallowed regions of the Ramachandran plot. Final refinement statistics are given in Table 1. Coordinates for the 2′-d-3′-AMP·PP_i·Mg^{2+} and 2′,5′-dd-3′-ATP·Mg^{2+} complexes have been deposited in the Protein Data Bank with the codes 1CS4 and 1CUL, respectively.

RESULTS

Crystal Structures of 2′-d-3′-AMP·PP_i Complexes. The structure of a complex of C_{1a}·C_{2a}·$G_s\alpha$ with 2′-d-3′-AMP·PP_i·Mg^{2+} at 2.8 Å resolution was previously reported (*2*). The inhibitor binds in the interface between the C_{1a} and C_{2a} domains and interacts with conserved residues known to be involved in catalysis, ATP binding, and P-site inhibition (*25*). It was hypothesized that ATP binds in a similar fashion, and a model of ATP was docked into the active site such that its purine ring superimposed with that of 2′-d-3′-AMP, and its β and γ phosphates superimposed with those of PP_i. This model was later corroborated by site-directed mutagenesis (*26*, *27*) and further refined by the recent structures of C_{1a}·C_{2a}·$G_s\alpha$ complexed with the competitive ATP analogues, β-L-2′,3′-dideoxyadenosine 5′-triphosphate and ATPαS (R_p) (*28*). In these structures, it was conclusively shown that two metal ions, called A and B, bind in the active site of adenylyl cyclase and that these metal sites have a preference for Zn^{2+} and Mn^{2+}, respectively, over the presumed physiological metal Mg^{2+}. Zn^{2+} is an inhibitor of adenylyl cyclase with an IC_{50} of 15 μM, whereas Mn^{2+} is an activator that typically increases the activity of C_{1a}·C_{2a}·$G_s\alpha$ 10-fold. Metals A and B play important roles in binding ATP and in catalysis. On the basis of modeling studies (*28*), metal A coordinates and reduces the pK_a of the 3′-hydroxyl of ATP, the nucleophile of the adenylyl cyclase reaction. Metal B coordinates and shields the developing negative charge of the leaving group (PP_i). Both metals are expected to stabilize the pentavalent transition state of the reaction by coordinating the pro-R oxygen of the α-phosphate.

Only metal B was observed in previous structure determinations of adenylyl cyclase complexed with 2′-d-3′-AMP·PP_i. A second metal might be expected to be present because adenylyl cyclase and certain other enzymes that catalyze phosphoryl transfer use a two metal ion mechanism (*29*, *30*). Furthermore, the 3′-phosphate of 2′-d-3′-AMP is in close proximity to PP_i and two aspartic acid side chains and a metal cation seems necessary to complement the excess negative charge. It is possible that the lower resolution (2.8 Å) of the previous structure determination was insufficient to reveal metal A. To examine this issue in more detail, we have determined higher resolution structures of this inhibitor bound to adenylyl cyclase in the presence of three different metal ions. Because Zn^{2+} preferentially binds in the metal A site when adenylyl cyclase is complexed with ATP analogues (*28*), Zn^{2+} was used in one of the structure determinations in an attempt to enhance electron density at site A. The structure of the complex was also determined in the presence of Mn^{2+}. Enhanced density at site B would help explain the lower K_d and increased potency of P-site inhibitors in the presence of this activating cation.

However, metal B is likewise the only metal observed in the three structures of the 2′-d-3′-AMP·PP_i complex reported here. There are no significant electron density peaks in a difference Fourier map generated between the 2′-d-3′-AMP·PP_i·Zn^{2+} and 2′-d-3′-AMP·PP_i·Mg^{2+} data sets, and there is no electron density or room in the active site for metal A. There are also no significant electron density peaks in the difference Fourier map between the 2′-d-3′-AMP·PP_i·Mn^{2+} and 2′-d-3′-AMP·PP_i·Mg^{2+} data sets. This seems to indicate that Mn^{2+} does not replace Mg^{2+} at site B in the complex with this inhibitor. Because Mn^{2+} is more electron dense than Mg^{2+}, any mixture of Mn^{2+} + Mg^{2+} at site B should

have resulted in a positive peak in the $Mn^{2+} - Mg^{2+}$ difference map. The observed lack of difference density indicates that the mole fraction of Mn^{2+} is low at this site. However, the metal ion specificity observed in complexes with competitive inhibitors still leads us to expect that Mn^{2+} activates adenylyl cyclase for P-site inhibition by binding at the metal B site and coordinating PP_i more tightly than would Mg^{2+}. Mn^{2+} could also enhance inhibition by accelerating production of PP_i, the coinhibitor, in addition to lowering the K_d of the inhibitor. We may be unable to observe binding of Mn^{2+} at the metal B site because the C_{1a}·C_{2a}·$G_s\alpha$ complex used for our experiments was isolated in the presence of forskolin, and Mn^{2+} has negligible effect on the potency of P-site inhibition under these conditions (see below).

Biochemical Studies of 2′,5′-dd-3′-ATP with Soluble Adenylyl Cyclase. 2′,5′-dd-3′-ATP is one of the most potent P-site inhibitors known with an IC_{50} of 40 nM against native adenylyl cyclase from rat brain in the presence of Mn^{2+} (*12*, *15*). Its mode of inhibition is either noncompetitive or uncompetitive, depending on the conditions of enzyme activation, and 2′,5′-dd-[γ-^{32}P]-3′-ATP has been demonstrated to bind directly to native adenylyl cyclases (*31*).[2] It is important to assess the ability of this ligand to bind and inhibit the recombinant C_{1a} and C_{2a} proteins used for our crystallographic studies and to assess competition with ATP analogues, PP_i, or cAMP.

Inhibition of the $G_s\alpha$-stimulated activity of the C_{1a} and C_{2a} cytoplasmic domains of adenylyl cyclase by 2′,5′-dd-3′-ATP was noncompetitive with respect to Mg^{2+}·ATP and exhibited an apparent K_i of 4 μM (Figure 2). The 100-fold decrease in affinity of 2′,5′-dd-3′-ATP for the C_{1a}:C_{2a} complex relative to that for native enzyme might be attributed to the absence in the latter of a covalent linkage between domains, and of other missing polypeptide segments that may promote interactions between domains in the native enzyme. This kinetic behavior is nevertheless consistent with that demonstrated previously with native and recombinant wild-type enzyme (*15*). Native and recombinant wild-type adenylyl cyclases exhibit an apparent high affinity for 2′,5′-dd-3′-ATP [IC_{50} 40−280 nM (*12*, *15*, *32*)], which can be measured by a filtration binding assay using 2′,5′-dd-[γ-^{32}P]-3′-ATP (*31*).[2] However, because of the comparatively high K_d of the C_{1a}·C_{2a} complex [$K_d \approx 1$ μM (*14*)] and the accordingly higher K_i for inhibition of these domains, equilibrium dialysis was used to quantify binding of 2′,5′-dd-[γ-^{32}P]-3′-ATP to the C_{1a}·C_{2a} complex in the presence of $G_s\alpha$ and Mg^{2+} (Figure 3). Binding of 2′,5′-dd-[γ-^{32}P]-3′-ATP with the C_{1a}·C_{2a} complex in the absence of PP_i was consistent with a noncompetitive pattern of inhibition. Inclusion of forskolin increased inhibitor binding (Figure 3), which was similar to results previously described for [^{3}H]2′-d-Ado (*14*). Binding of 2′,5′-dd-[γ-^{32}P]-3′-ATP required both C_{1a} and C_{2a} and was not observed with the individual domains at the protein concentrations tested. Previous covalent labeling experiments with the irreversibly binding affinity probe, 2′,5′-dideoxyadenosine 3′-[γ-(1-methylimidizole)-triphosphate], suggested that the inhibitor interacts with individual C_{1a} and C_{2a} domains (*17*). However, no binding of 2′,5′-dd-[γ-^{32}P]-3′-ATP could be detected by equilibrium dialysis using the individual domains, despite the inclusion of Mg^{2+}, Mn^{2+} or Mg^{2+}·PP_i.

For enzyme activated with $G_s\alpha$, binding of 2′,5′-dd-[γ-^{32}P]-3′-ATP was approximately 2-fold greater in the presence of Mn^{2+} than with Mg^{2+} (Figures 3 and 4). However, for enzyme activated with $G_s\alpha$ and forskolin, Mn^{2+} had a much smaller effect. The K_d for binding 2′,5′-dd-[γ-^{32}P]-3′-ATP was significantly lower in the presence of Mn^{2+} (0.2 μM versus 2.4 μM with Mg^{2+}), as determined by Scatchard analysis with only a single molecule of inhibitor binding per molecule of adenylyl cyclase (Figure 4).

Competition between 2′,5′-dd-3′-ATP and ATP analogues, P-site inhibitors and cAMP are consistent with the binding of 2′,5′-dd-3′-ATP at the active site. In contrast, PP_i enhances binding of the inhibitor (Figures 3 and 5). Consistent with the requirement for PP_i for inhibition of adenylyl cyclases by adenine nucleosides and adenine nucleoside monophosphates, inhibition of 2′,5′-dd-[γ-^{32}P]-3′-ATP binding by 2′-d-3′-AMP was also enhanced by PP_i (Figure 5). Further, a Dixon plot of 1/velocity versus the concentration of PP_i at different fixed concentrations of 2′,5′-dd-3′-ATP yields a family of intersecting lines above the [PP_i] axis (Figure 6). The increase in binding noted with PP_i has consistently been demonstrated in experiments with the C_{1a}·C_{2a} complex, as shown here, as well as with native and recombinant wild-type enzyme (*31*).[2] These observations suggest paradoxically that both 2′,5′-dd-3′-ATP and PP_i bind adenylyl cyclase simultaneously.

Crystal Structures of 2′,5′-dd-3′-ATP Complexes. As for the three complexes of 2′-d-3′-AMP·PP_i, no significant peaks appeared in the difference Fourier maps computed with the data set for the 2′,5′-dd-3′-ATP·Mg^{2+} complex with respect to that for either 2′,5′-dd-3′-ATP·Mn^{2+} or 2′,5′-dd-3′-ATP·Zn^{2+}. This result appears contrary to the observation that Mn^{2+} enhanced P-site inhibition by 2′,5′-dd-3′-ATP (Figures 3 and 4). However, because forskolin was included in the formation of the ternary complex of C_{1a}·C_{2a}·$G_s\alpha$ used for our crystal studies, there may be no dramatic difference in the affinity of the metal B site for Mg^{2+} and that for Mn^{2+} (Figure 3). The absence of any noticeable difference peaks for Zn^{2+} again indicates that the metal A site, if extant, has no apparent preference for either Zn^{2+} or Mn^{2+}. Mg^{2+} apparently predominates at both sites, despite the fact that it was not specifically included in the soaks for Zn^{2+} or Mn^{2+}. Alternatively, Zn^{2+} or Mn^{2+} may be bound at such a low mole fraction that they are indistinguishable from a fully occupied Mg^{2+}.

The electron density omit map for 2′,5′-dd-3′-ATP·Mn^{2+} bound to adenylyl cyclase is shown in Figure 1B. A single model of the inhibitor could not be fit into the electron density with reasonable stereochemistry. Therefore, the inhibitor was modeled as the structurally overlapping fragments 2′,5′-dd-3′-AMP and triphosphate. The 3′ phosphate of 2′,5′-dd-3-AMP and the α-phosphate of triphosphate both correspond to the α-phosphate of 2′,5′-dd-3′-ATP and are partially overlapping. The ligand therefore appears to exhibit static disorder such that it contacts the enzyme either via its triphosphate tail or its nucleoside moiety, but neither at the same time. After refinement of this model for the 2′,5′-dd-3′-ATP·Mn^{2+} complex, the average temperature factors of forskolin and GTPγS (which is bound in the active site of $G_s\alpha$) are 33 and 32 Å^2, respectively. Both are assumed to bind at 100% occupancy. The average temperature factor of the 2′,5′-dd-3′-AMP fragment is 37 Å^2, suggesting nearly

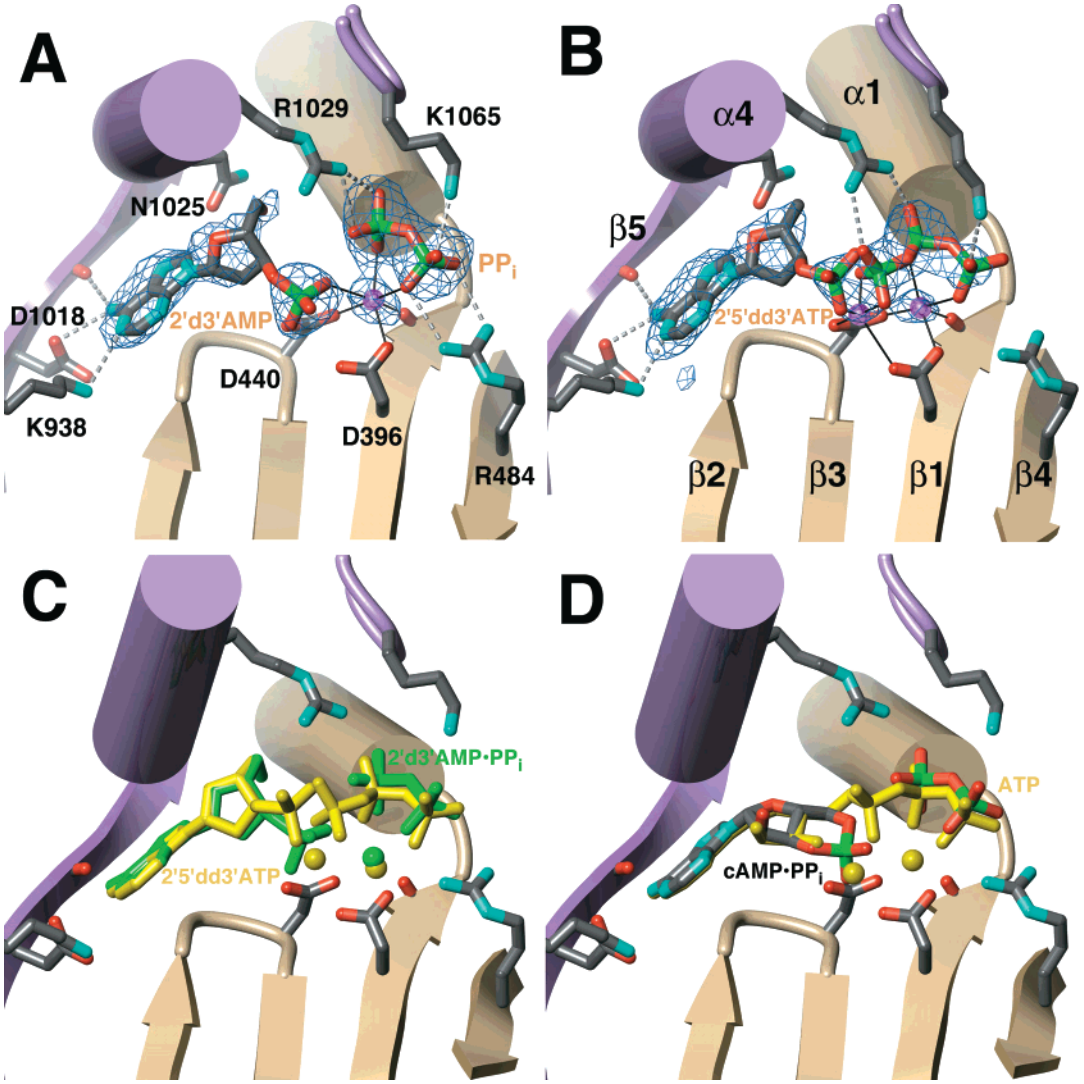

FIGURE 1: Complexes of adenylyl cyclase with P-site inhibitors. (A) Complex of 2′-d-3′-AMP·PP_i with the catalytic core of adenylyl cyclase. 2′-d-3′-AMP·PP_i binds in the active site of adenylyl cyclase, within the cleft between the C_{1a} and C_{2a} domains. Protein side chains and 2′-d-3′-AMP and PP_i molecules are drawn as stick models. Thin black lines depict the octahedral coordination of the metal ion, which is shown as a metallic magenta sphere. Structural elements donated to the active site by the C_{1a} and C_{2a} domains of adenylyl cyclase are shown in tan and mauve, respectively. Carbon atoms are gray, nitrogens blue, oxygens red, and phosphorus green. Amino acids are labeled according to their position in canine type V adenylyl cyclase for C_{1a} and rat type II adenylyl cyclase for C_{2a}. The blue wire cage corresponds to electron density from a 2.5 Å resolution $|F_{o_{Zn}}| - |F_c|$ omit map contoured at 3σ. (B) Complex of 2′,5′-dd-3′-ATP with the catalytic core of adenylyl cyclase. 2′,5′-dd-3′-ATP cannot be modeled into the observed electron density, and thus was modeled as two fragments: 2′,5′-dd-3′-AMP and triphosphate. The structure suggests that there are two binding modes for the inhibitor, the first via its nucleoside, and the second via its triphosphate tail. Two metals bind concurrently with the inhibitor (magenta). Metal A has only four obvious ligands while metal B has five. Secondary structure is labeled as defined previously (*2*). The blue wire cage corresponds to electron density from a 2.4 Å resolution $|F_{o_{Mn}}| - |F_c|$ omit map contoured at 3σ. (C) Superposition of 2′-d-3′-AMP·PP_i (green) and 2′,5′-dd-3′-AMP/triphosphate (yellow) within the active site of adenylyl cyclase. Due to its smaller 5′ substituent, the ribose ring of 2′,5′-dd-3′-AMP binds deeper in a pocket formed between the α2 and α4 helices. In addition, its 3′-phosphate is further away from D440, allowing metal A to bind. The view is rotated 20° around a vertical axis with respect to panels A and B. (D) Model of the cAMP·PP_i complex of adenylyl cyclase. The structure of cAMP is based on three high-resolution crystal structures (*35*−*37*), and was positioned by superimposing its purine and ribose rings on those of a model of ATP (yellow) in the active site (*28*). PP_i is the same as in the 2′-d-3′-AMP structure. The phosphate of cAMP is within 1 Å of the binding site of the 3′ phosphate of 2′-d-3′-AMP. As modeled, the phosphate of cAMP is too close to the carboxyl side chain of D440 and the cyclic phosphate ring will probably have a different pucker in the true enzyme·product complex. Therefore, the energetically preferred conformation of cAMP, if it indeed corresponds to that found in small molecule crystal structures, is not compatible with the active site. Such would explain why cAMP leaves the active site before PP_i, allowing P-site inhibitors such as 2′-d-3′-AMP to later bind and lock the enzyme in a dead-end complex.

complete occupancy. Hence, when binding by its nucleoside moiety, the triphosphate tail of 2′,5′-dd-3′-ATP is poorly ordered and probably lies along the same general path as the triphosphate fragment. The average temperature factor for triphosphate is 89 $Å^2$, indicating much greater disorder or much lower occupancy.

The fact that 2′,5′-dd-3′-ATP exhibits static disorder upon binding to adenylyl cyclase might reflect the inability of the crystalline enzyme, composed of truncated domains from two adenylyl cyclase isozymes, to attain a "fully closed" conformation. A partially open active site would thus not allow the nucleoside and pyrophosphate moieties of the inhibitor

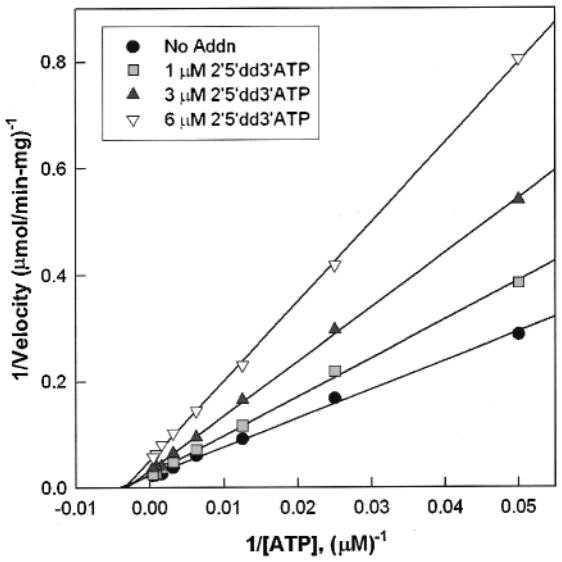

FIGURE 2: Noncompetitive inhibition of $G_s\alpha$-stimulated adenylyl cyclase activity by 2′,5′-dd-3′-ATP. Assays [0.7 nM C_{1a}(591), 1 μM C_{2a}, 0.4 μM GTPγS−$G_s\alpha$] were performed in the presence of 10 mM free $MgCl_2$, 0.02−2.56 mM MgATP, and either 0 (●), 1 (■), 3 (▲), or 6 (▼) μM 2′,5′-dd-3′-ATP. The apparent K_i (4 μM) was determined by Lineweaver−Burk analysis.

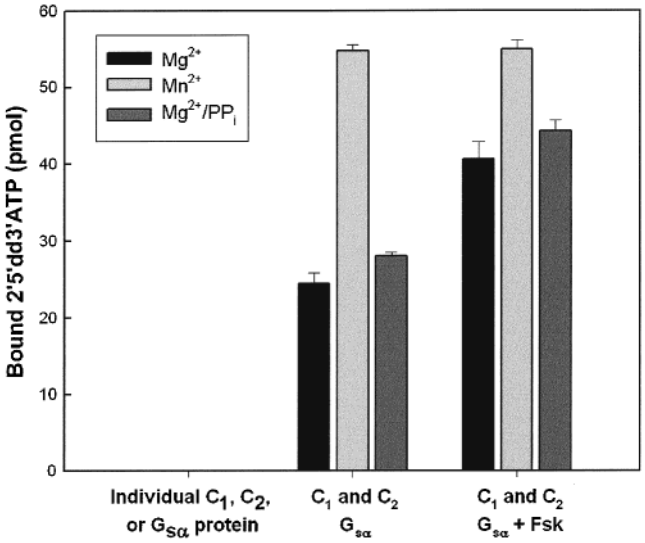

FIGURE 3: Binding of 2′,5′-dd-[γ-^{32}P]-3′-ATP to adenylyl cyclase. The individual proteins (10 μM) C_{1a}(591), C_{2a}, or GTPγS−$G_s\alpha$ were incubated with 1.5 μM 2′,5′-dd-[γ-^{32}P]-3′-ATP for 24 h at 4° C. Equilibrium dialysis was performed in the presence of either 4 mM $MgCl_2$, 2 mM $MnCl_2$, or 4 mM $MgCl_2$ and 2 mM PP_i. Binding of 2′,5′-dd-[γ-^{32}P]-3′-ATP was also measured in the presence of all three proteins [2 μM C_{1a}(591), C_{2a}, and GTPγS−$G_s\alpha$] in the presence or absence of 100 μM forskolin. Results shown are representative of two experiments.

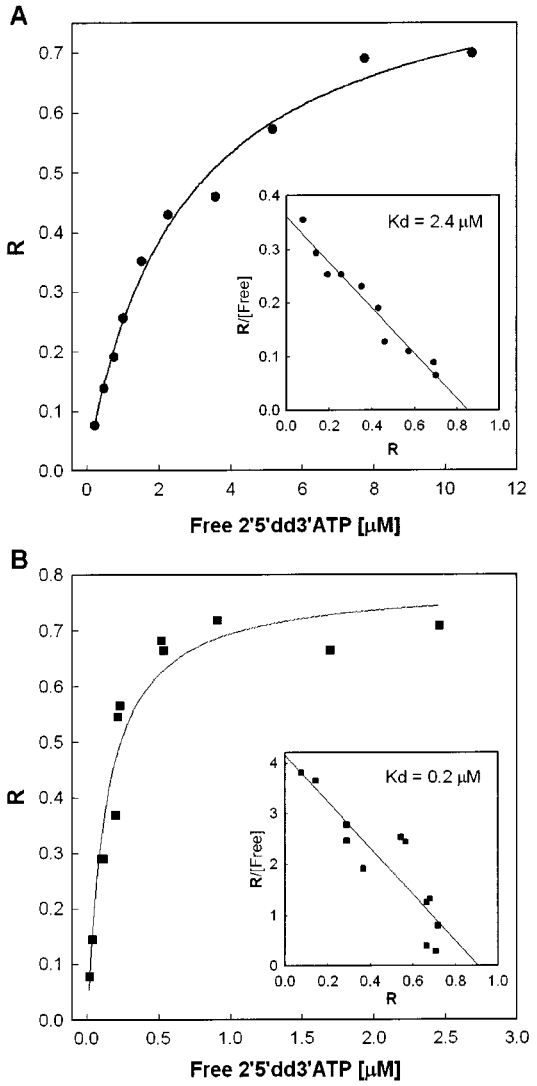

FIGURE 4: Binding of 2′,5′-dd-[γ-^{32}P]-3′-ATP to adenylyl cyclase in the presence of Mg^{2+} or Mn^{2+}. C_{1a}, C_{2a}, and GTPγS−$G_s\alpha$ were incubated with 0.1−12.8 μM 2′,5′-dd-[γ-^{32}P]-3′-ATP for 24 h as described under Experimental Procedures. (A) equilibrium dialysis reactions contained 4 μM of each protein and 5 mM $MgCl_2$. (B) reactions contained 2 μM of each protein and 2.5 mM $MnCl_2$. Dissociation constants were calculated by Scatchard analysis (insets). The relative amount of bound 2′,5′-dd-3′-ATP (R) represents the total concentration of bound ligand divided by the total concentration of active adenylyl cyclase. These results are representative of three experiments.

to bind simultaneously (their respective sites are 1−2 Å too far apart in the refined structure). However, the kinetic data supports the observed static disorder. First, PP_i does not compete with, but rather augments binding of 2′,5′-dd-[γ-^{32}P]-3′-ATP (Figure 3,5). This is consistent with the observed electron density, which suggests that the triphosphate of 2′,5′-dd-3′-ATP binds with low affinity and, therefore, could easily be displaced by PP_i. Second, the greater potency of 2′,5′-dd-3′-A4P ($IC_{50} \approx 7.4$ nM) compared with the corresponding 3′-triphosphate ($IC_{50} \approx 40$ nM) (*33*) is consistent with an active site large enough to accommodate a tetraphosphate. In the active site of the 2′,5′-dd-3′-ATP complex, there is room for a fourth phosphate. This would not be possible if the active site were compressed such that it could accommodate 2′,5′-dd-3′-ATP in a single binding mode.

After refinement of the model for the statically disordered 2′,5′-dd-3′-ATP complex, a weak (1−2 standard deviations above he mean value of he map) peak was observed in the $|F_o - F_c|$ difference Fourier map—close to the position of metal A seen in complexes with ATP analogues. The peak was modeled as Mg^{2+} and is located 2 Å from the oxygen substituents of both the 3′-phosphate of 2′,5′-dd-3′-AMP fragment and the triphosphate α phosphate. The metal is also coordinated by D396 and D440 (Figure 1B). Thus, the number of observed ligands is less than four. Poorly ordered water molecules could serve as additional ligands.

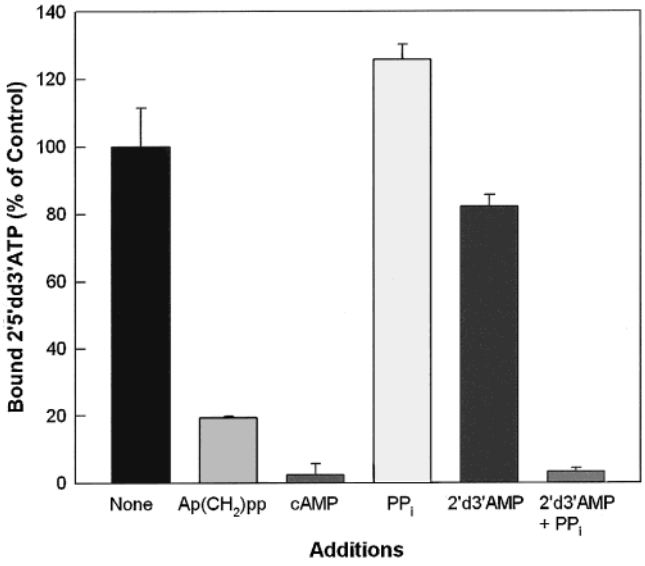

FIGURE 5: Competition for the binding of 2′,5′-dd-[γ-^{32}P]-3′-ATP to adenylyl cyclase. C_{1a}(591), C_{2a}, and GTPγS−$G_s\alpha$ (4 μM) were incubated with 0.08 μM 2′,5′-dd-[γ-^{32}P]-3′-ATP in the presence of 5 mM $MgCl_2$. Competition for binding by equilibrium dialysis was performed with 6 mM Mg^{2+}·AP(CH_2)PP, 25 mM cAMP, 2 mM Mg^{2+}·PP_i, 400 μM 2′-d-3′-AMP, or 2′-d-3′-AMP (400 μM) and Mg^{2+}·PP_i (2 mM). Results shown are representative of three experiments.

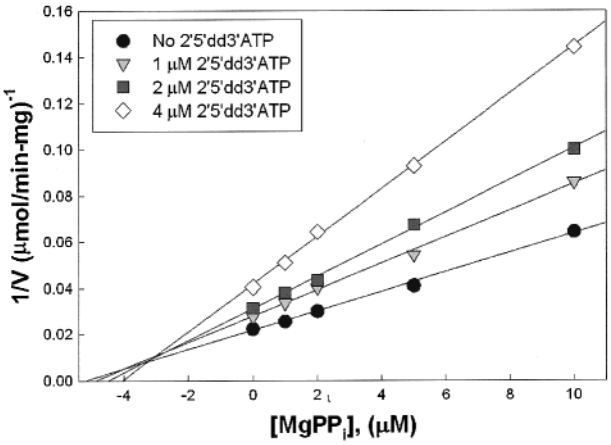

FIGURE 6: Dixon plot of PP_i and 2′5′-dd-3′-ATP inhibition of adenylyl cyclase activity. Assays [4 nM C_{1a}(591) and 1 uM C_{2a}] were preformed in the presence of 10 mM free $MgCl_2$, 1 mM ATP, and 400 nM activated Gsα. The indicated concentrations of Mg−PP_i and 2′5′-dd-3′-ATP were added and the reaction was incubated at 30 °C for 10 min.

DISCUSSION

The crystal structures reported here allow speculation on the molecular basis of the relative potency of P-site inhibitors. All P-site inhibitors require an intact adenine ring, reflecting the fact that their purine rings use the same binding pocket as the substrate ATP. The removal of 2′ and 5′ hydroxyl groups from P-site ligands enhances their potency by 7−200-fold, depending on other modifications (*4*, *12*, *15*). These deletions remove potential collisions of the 2′-hydroxyl with nearby protein superstructure. A 2′-hydroxyl group in the structure of the 2′-d-3′-AMP·PP_i complex (Figure 1A) would collide with the side chain of D440 and the backbone carbonyl of residue 438. This may be reflected in the reduced potency of 3′-AMP ($IC_{50} \approx 9$ μM) compared with 2′-d-3′-AMP ($IC_{50} \approx 2.7$ μM) reported for native enzyme (*4*). Ribose rings with less substitution are inherently more flexible than their fully substituted counterparts. Therefore, 2′-deoxy and 2′,5-dideoxy ribose groups and especially acyclic adenine derivatives (*34*) would allow the inhibitor to adopt conformations that better conform to the active site. Such flexibility may be especially important when the inhibitor has a bulky 3′-substitution as does 2′,5′-dd-3′-ATP.

Comparison of the 2′-d-3′-AMP·PP_i structure with that of 2′,5′-dd-3′-ATP yields further insights (Figure 1C). Compounds with ribose rings lacking 5′-hydroxyl groups inhibit 2−7 times more efficaciously than their substituted counterparts. From the structures reported here, the removal of a 5′-oxygen allows the ribose ring to slip further back into the nucleoside binding pocket, where the 5′-methylene groups packs against helix α4 of C_{2a}. This interaction is apparently more favorable than maintenance of a hydrogen bond between the 5′-hydroxyl and the side chain of Thr401, as occurs in the 2′-d-3′-AMP·PP_i structure.

Adenine-nucleoside 3′-polyphosphates are the most potent P-site ligands, with the successive addition of phosphate groups to the 3′-position adding substantially to potency: 2′,5′-dd-3′-AMP ($IC_{50} \approx 460$ nM), 2′,5′-dd-3′-ATP ($IC_{50} \approx$ 40 nM); 2′,5′-dd-3′-A4P ($IC_{50} \approx 7.4$ nM) with native enzyme (*12*, *15*, *33*). These potencies are consistent with each successive phosphate contributing ∼2−4 kcal of binding energy. On the basis of the 2′,5′-dd-3′-ATP structure reported here, 3′-polyphosphate inhibitors are statically disordered in the active site with the 3′-polyphosphate being most poorly ordered. However, 3′-polyphosphates could enhance inhibition in a number of other ways besides contribution of binding energy. First, the polyphosphate group can interact with and neutralize the positive charges in the active site. Second, the polyphosphate could stabilize the enzyme in a closed conformation required for tight binding of the adenosine moiety of the inhibitor. Finally, 3′-polyphosphate moieties can be thought of as covalently linked PP_i "tags". P-site inhibitors that possess such tags will have an entropic advantage, arising from approximation of functional moieties, over inhibitors that require binding of two separate molecules (e.g., 2′-d-3′-AMP·PP_i) for effective inhibition.

The α-phosphate group of 2′,5′-dd-3′-ATP occupies a different position from that in 2′-d-3′-AMP (Figure 1C). As a consequence, the α-phosphate of the latter inhibitor occludes metal ion site A. Therefore, P-site inhibitors with 3′-polyphosphates could also be more potent because they bind concurrently with two metal ions. The extra metal helps to neutralize excess negative charge in the active site such as that found in the 2′-d-3′-AMP·PP_i complex. The weak electron density observed for metal A in the 2′,5′-dd-3′-ATP complex could result from static disorder of the inhibitor.

The relatively low affinity P-site inhibitors 2′-d-Ado and 2′-d-3′-AMP display uncompetitive inhibition with respect to ATP in the presence of $G_s\alpha/Mg^{2+}$ and exhibit noncompetitive inhibition when adenylyl cyclase is activated by Mn^{2+} (*13*, *14*). In either case, these inhibitors are believed to bind to the enzyme as an enzyme·PP_i·inhibitor complex. The noncompetitive inhibition exhibited by 2′,5′-dd-3′-ATP may reflect its ability to bind to both the free enzyme and the enzyme·PP_i complex. Although there is no direct evidence for the simultaneous binding of 2′,5′-dd-3′-ATP and PP_i, the observation that pyrophosphate enhances binding

of 2′,5′-dd-[γ-^{32}P]-3′-ATP suggests that this may occur. In this scenario, PP_i would displace the poorly ordered β and γ phosphates of 2′,5′-dd-3′-ATP. Alternatively, synergistic activity of PPi could be due to hysteretic behavior of the enzyme, such that the active conformation promoted by PPi might persist after that ligand dissociates and thereby favor subsequent binding of 2′,5′-dd-3′-ATP.

In contrast, 2′,5′-dd-3′-ATP in the presence of Mn^{2+} could be classified as an inactivator of adenylyl cyclase. If the binding of 2′,5′-dd-3′-ATP·Mn^{2+} traps a fraction of adenylyl cyclase in a dead-end complex, an apparent noncompetitive pattern of inhibition will result because the effective total enzyme concentration (and hence υ_{max}) is reduced while K_m is unchanged.

It seems clear from its uncompetitive mode of inhibition, its requirement for PP_i, and its ability to inhibit the reverse reaction of adenylyl cyclase competitively that the typical P-site inhibitor is essentially a cAMP analogue that binds to the enzyme before the second product PP_i is released (*14*). By comparison, P-site inhibitors with 3′ polyphosphates appear to function as covalently linked analogues of cAMP and PP_i, whose greater affinity arises in part from their inherent entropic benefits. By superimposing the structure of cAMP onto that of 2′-d-3′-AMP (Figure 1D), we can generate a reasonable model for the enzyme·product complex for activated adenylyl cyclase which we can compare to the model for the enzyme·substrate complex (*28*). Unlike P-site inhibitors, which adopt 2′-endo, 3′-exo ribose conformations, cAMP is constrained in the 3′-endo, 2′-exo conformation. To facilitate nucleophilic attack of the 3′-hydroxyl upon the 5′-phosphate, ATP must also adopt a 3′-endo conformation in the activated complex, and its polyphosphate backbone must adopt a conformation that brings O3′ within van der Waals contact distance of the 5′-phosphate. This may engender some steric strain. The 3′-polyposphate backbone of 2′-d-3′-ATP and the 3′-monophosphate of 2′-d-3′-AMP in conjunction with PP_i are able to occupy the active site without internal strain and therefore are efficacious inhibitors. These models, developed with truncated chimeric constructs, provide an excellent starting point for the rational development of conformation-selective drugs that are specific for native adenylyl and guanylyl cyclases.

ACKNOWLEDGMENT

We thank Julie Collins for superb technical assistance and the staff at the Cornell High Energy Synchrotron Source for assistance with data collection.

REFERENCES

1. Zhang, G., Liu, Y., Ruoho, A. E., and Hurley, J. H. (1997) *Nature 386*, 247−253.
2. Tesmer, J. J. G. T., Sunahara, R. K., Gilman, A. G., and Sprang, S. R. (1997) *Science 278*, 1907−1916.
3. Londos, C., and Wolff, J. (1977) *Proc. Natl. Acad. Sci. U.S.A. 74*, 5482−5486.
4. Johnson, R. A., Yeung, S. M., Stubner, D., Bushfield, M., and Shoshani, I. (1989) *Mol. Pharmacol. 35*, 681−688.
5. Wolff, J., Londos, C., and Cook, G. H. (1978) *Arch. Biochem. Biophys. 191*, 161−168.
6. Premont, J., Guillon, G., and Bockaert, J. (1979) *Biochem. Biophys. Res. Commun. 90*, 513−519.
7. Neer, E. J., and Salter, R. S. (1981) *J. Biol. Chem. 256*, 12102−12107.
8. Florio, V., and Ross, E. (1983) *Mol. Pharmacol. 24*, 195−202.
9. Johnson, R. A., Jakobs, K. H., and Schultz, G. (1985) *J. Biol. Chem. 260*, 114−121.
10. Dessauer, C. W., and Gilman, A. G. (1996) *J. Biol. Chem. 271*, 16967−16974.
11. Bushfield, M., Shoshani, I., and Johnson, R. A. (1990) *Mol. Pharmacol. 38*, 848−853.
12. Désaubry, L., Shoshani, I., and Johnson, R. A. (1996) *J. Biol. Chem. 271*, 14028−14034.
13. Johnson, R. A., and Shoshani, I. (1990) *J. Biol. Chem. 265*, 11595−11600.
14. Dessauer, C. W., and Gilman, A. G. (1997) *J. Biol. Chem. 272*, 27787−27795.
15. Désaubry, L., Shoshani, I., and Johnson, R. A. (1996) *J. Biol. Chem. 271*, 2380−2382.
16. Dessauer, C. W., Tesmer, J. J., Sprang, S. R., and Gilman, A. G. (1999) *Trends Pharmacol. Sci. 20*, 205−210.
17. Doronin, S., Murray, L., Dessauer, C. W., and Johnson, R. A. (1999) *J. Biol. Chem. 274*, 34745−34750.
18. Graziano, M. P., Freissmuth, M., and Gilman, A. G. (1989) *J. Biol. Chem. 264*, 409−418.
19. Sunahara, R. K., Dessauer, C. W., Whisnant, R. E., Kleuss, C., and Gilman, A. G. (1997) *J. Biol. Chem. 272*, 22265−22271.
20. Lee, E., Linder, M., and Gilman, A. (1994) *Methods Enzymol 237*, 146−164.
21. Garbers, D. L., and Johnson, R. A. (1975) *J. Biol. Chem. 250*, 8449−8456.
22. Dessauer, C. W., Scully, T. T., and Gilman, A. G. (1997) *J. Biol. Chem. 272*, 22272−22277.
23. Bailey, S. (1994) *Acta Crystallogr., Sect. D 50*, 760−763.
24. Brünger, A. T., Adams, P. D., Clore, G. M., DeLano, W. L., Gros, P., Grosse-Kunstleve, R. W., Jiang, J. S., Kuszewski, J., Nilges, M., Pannu, N. S., Read, R. J., Rice, L. M., Simonson, T., and Warren, G. L. (1998) *Acta Crystallogr., Sect. D 54*, 905−921.
25. Tang, W.-J., Stanzel, M., and Gilman, A. G. (1995) *Biochemistry 34*, 14563−14572.
26. Sunahara, R. K., Beuve, A., Tesmer, J. J. G., Sprang, S. R., Garbers, D. L., and Gilman, A. G. (1998) *J. Biol. Chem. 273*, 16332−16338.
27. Tucker, C. L., Hurley, J. H., Miller, T. R., and Hurley, J. B. (1998) *Proc. Natl. Acad. Sci. U.S.A 95*, 5993−5997.
28. Tesmer, J. J., Sunahara, R. K., Johnson, R. A., Gosselin, G., Gilman, A. G., and Sprang, S. R. (1999) *Science 285*, 756−760.
29. Kim, E. E., and Wyckoff, H. W. (1991) *J. Mol. Biol. 218*, 449−464.
30. Steitz, T. A., Smerdon, S. J., Jäger, J., and Joyce, C. M. (1994) *Science 266*, 2022−2025.
31. Napolitano, B. C., Murray, L., Szczepanik, M., and Johnson, R. A. (1998) *Faseb. J. 12*, A1478.
32. Johnson, R. A., Désaubry, L., Bianchi, G., Shoshani, I., Lyons E, J., Taussig, R., Watson, P. A., Cali, J. J., Krupinski, J., Pieroni, J. P., and Iyengar, R. (1997) *J. Biol. Chem. 272*, 8962−8966.
33. Désaubry, L., and Johnson, R. A. (1998) *J. Biol. Chem. 273*, 24972−24977.
34. Shoshani, I., Laux, W. H., C, P. r., Gosselin, G., and Johnson, R. A. (1999) *J. Biol. Chem. 274*, 34742−34744.
35. Varughese, K. I., Lu, C. T., and Kartha, G. (1982) *J. Am. Chem. Soc. 104*, 3398.
36. Padmaja, N., Ramakumar, S. R., and Viswamitra, M. A. (1991) *Bull. Chem. Soc. Jpn. 64*, 1359.
37. Sheldrick, W. S., and Rieke, E. (1978) *Acta Crystallogr., Sect. B 34*, 2324.

BI0015562